

Fred Cooper ಠ ; Avinash Khare 💿 ; John F. Dawson 💿 ; Efstathios G. Charalampidis 🕶 💿 ; Avadh Saxena 👨



Chaos 34, 043138 (2024) https://doi.org/10.1063/5.0183167







Chaos

Focus Issue:

Intelligent Game on Networked Systems: Optimization, Evolution and Control

Guest Editors: Lin Wang, Yang Lou, Zhihai Rong, and Guanrong Chen

Submit Today





The application of the "inverse problem" method for constructing confining potentials that make N-soliton waveforms exact solutions in the Gross-Pitaevskii equation

Cite as: Chaos **34**, 043138 (2024); doi: 10.1063/5.0183167 Submitted: 21 October 2023 · Accepted: 26 December 2023 · Published Online: 15 April 2024







Fred Cooper,^{1,2,a)} Avinash Khare,^{3,b)} John F. Dawson,^{4,c)} Efstathios G. Charalampidis,^{5,d)} and Avadh Saxena^{2,e)}

AFFILIATIONS

- ¹Santa Fe Institute, 1399 Hyde Park Road, Santa Fe, NM 87501, USA
- ²Center for Nonlinear Studies and Theoretical Division, Los Alamos National Laboratory, Los Alamos, NM 87545, USA
- ³Physics Department, Savitribai Phule Pune University, Pune 411007, India
- ⁴Department of Physics, University of New Hampshire, Durham, NH 03824, USA
- ⁵Mathematics Department, California Polytechnic State University, San Luis Obispo, CA 93407-0403, USA

Note: This paper is part of the Focus Issue on Topics in Nonlinear Science: Dedicated to David K. Campbell's 80th Birthday.

- a) Electronic mail: cooper@santafe.edu
- b) Electronic mail: avinashkhare 45@gmail.com
- c) Electronic mail: john.dawson@unh.edu
- $^{
 m d)}$ Author to whom correspondence should be addressed: echarala@calpoly.edu
- e)Electronic mail: avadh@lanl.gov

ABSTRACT

In this work, we discuss an application of the "inverse problem" method to find the external trapping potential, which has particular N trapped soliton-like solutions of the Gross–Pitaevskii equation (GPE) also known as the cubic nonlinear Schrödinger equation (NLSE). This inverse method assumes particular forms for the trapped soliton wave function, which then determines the (unique) external (confining) potential. The latter renders these assumed waveforms exact solutions of the GPE (NLSE) for both attractive (g < 0) and repulsive (g > 0) self-interactions. For both signs of g, we discuss the stability with respect to self-similar deformations and translations. For g < 0, a critical mass M_c or equivalently the number of particles for instabilities to arise can often be found analytically. On the other hand, for the case with g > 0 corresponding to repulsive self-interactions which is often discussed in the atomic physics realm of Bose–Einstein condensates, the bound solutions are found to be always stable. For g < 0, we also determine the critical mass numerically by using linear stability or Bogoliubov–de Gennes analysis, and compare these results with our analytic estimates. Various analytic forms for the trapped N-soliton solutions in one, two, and three spatial dimensions are discussed, including sums of Gaussians or higher-order eigenfunctions of the harmonic oscillator Hamiltonian.

Published under an exclusive license by AIP Publishing. https://doi.org/10.1063/5.0183167

Understanding the behavior of trapped atoms in BECs requires the numerical study of the existence, stability, and spatiotemporal dynamics of solutions to the Gross-Pitaevskii equation (GPE). Exact solutions of the GPE subject to external potentials offer a path in which not only numerical simulations can be carried out for this purpose, but analytical estimates for the stability of coherent structures can be derived. In this work, we consider the inverse problem method, which is capable of determining suitable external potentials that make specified N-trapped soliton wave functions exact solutions to the GPE. The stability of these solutions is studied using Derrick's theorem and energy land-scape techniques. Moreover, we discuss potential realizations of

trapped BECs in 1D, 2D, and 3D. Our theoretical results on stability analysis are compared with spectral computations in the realm of Bogoliubov-de Gennes (BdG) analysis.

I. INTRODUCTION

The nonlinear Schrödinger equation (NLSE)1 has arguably been the focal point of studies in nonlinear models because its ubiquitous envelope equation arises in diverse physical contexts with a wide array of physical applications. Those include the description of the pulse propagation in nonlinear optical fibers,^{2,3} the evolution of the envelope of modulated wave groups,^{4,5} as well as the propagation of strongly dispersive waves in plasmas,6 among many others. When the NLSE incorporates an external, i.e., confining potential, it is often called the Gross-Pitaevskii equation (GPE), which is a fundamental model for describing the static and dynamical properties of atomic Bose-Einstein condensates (BEC) in the mean-field approximation.⁷⁻⁹ Indeed, solutions (either obtained analytically or numerically) of the related GPE in multiple well potentials are very useful in understanding the behavior of trapped atoms in BECs. Both signs of the self-interaction coupling constant can be implemented when studying BECs, by varying the external magnetic field near the Feshbach resonance. 10 Using such methods, attractive self-interaction solitons have been found in BECs.¹¹

There are various strategies for finding solutions to the GPE for given external potentials. Indeed, and for a given potential, one may linearize the GPE (i.e., upon neglecting the nonlinearity term therein) and obtain an eigenvalue problem for the (discrete) energy levels (eigenvalues) and quantum states (eigenfunctions) of the system. The resulting problem is of a Sturm-Liouville type, i.e., a linear Schrödinger equation, and may be solved either analytically¹² or numerically, see, e.g., Refs. 13 and 14. Its eigenvalues coincide with the values of the so-called chemical potential9 at which nonlinear states bifurcate from. Then, for each eigenvalue (i.e., value of the chemical potential at the linear limit) and respective linear state, one can continue the latter toward the nonlinear regime by varying the chemical potential which itself controls the number of atoms in a BEC. This departure from the linear limit is accomplished by using numerical continuation methods.¹⁵ Another strategy for finding solutions to the GPE revolves around starting with an approximate solution and then varying the potential to find a solution.

In the present article, we depart from these strategies and use the so-called "inverse problem" method. Within this method, one chooses beforehand a wave function that we wish to be an exact solution of the GPE, and determines what confining potential makes this a solution. This way, various external potentials can be constructed with an eye toward realizing them experimentally. This method has previously been used by Malomed and Stepanyants¹⁶ in the standard GPE to determine potentials that have exact Gaussian-like solutions. It has also been used in Ref. 17 for potentials in the GPE with arbitrary nonlinearity exponent. Recently, the authors of the present work have shown how to find confining potentials in the GPE which lead to constant density, flat-top solitons in one, two, and three dimensions (denoted hereafter as 1D, 2D, and 3D, respectively).¹⁸ Herein, we consider wave function Ansätze corresponding to *N*-soliton pulses and identify the respective potentials

that make them exact solutions to the GPE in 1D, 2D, and 3D. Moreover, and since the inverse problem method gives us exact solutions, we are able to provide analytic estimates for the critical mass for attractive self-interaction solitons above which the soliton becomes unstable. These are obtained by using Derrick's theorem¹⁹ or by studying the energy landscape for translation deformations of the soliton.¹⁷ We compare our analytical findings on stability of the soliton solutions against linear stability considerations by using the Bogoliubov–de Gennes^{20,21} (BdG) method.

The paper is structured as follows. In Sec. II, we present the main setup of the inverse problem method together with the linear response equations. Multi-soliton solutions in 1D, 2D, and 3D are discussed in Sec. III together with their response under self-similar and translational deformations. In Sec. IV, we study the linear response equations and compare our findings against numerical simulations. Finally, we state our conclusions in Sec. V.

II. INVERSE PROBLEM METHOD FOR THE CONFINING POTENTIAL AND THE LINEAR STABILITY OF THE SOLUTIONS

We consider herein a collection of particles with mass m=1/2 and contact interaction strength g which is described by a classical action. Upon confining the particles with the introduction of an external potential denoted as $V(r) \in \mathbb{R}$, the nonlinear Schrödinger or Gross–Pitaevskii equation (NLSE or GPE, respectively) for this system⁹ is then given by

$$\left\{-\nabla^2 + g|\psi(\mathbf{r},t)|^2 + V(\mathbf{r})\right\}\psi(\mathbf{r},t) = \mathrm{i}\partial_t\psi(\mathbf{r},t),\tag{1}$$

where $\psi(\mathbf{r},t)$ is a complex-valued function, i.e., $\psi(\mathbf{r},t) \in \mathbb{C}$. Here, we use units such that $\hbar = 1$ (see also Ref. 18). It should be noted in passing that in the absence of the external potential [i.e., $V(\mathbf{r}) \equiv 0$], soliton solutions exist for both repulsive (g > 0) interactions (see Ref. 22) and attractive (g < 0) interactions (see Ref. 23). The case of a non-zero constant potential can be added or even excluded since it can be removed by introducing a phase.

Suppose that $u_0(r) \in \mathbb{R}$ is the solution to Eq. (1) at t=0. If we assume a time-dependent solution for $\psi(r,t)$ given by the separation of variables ansatz

$$\psi(\mathbf{r},t) = u_0(\mathbf{r})e^{-i\omega t}, \qquad (2)$$

then Eq. (1) is written as

$$\omega u_0(\mathbf{r}) + \nabla^2 u_0(\mathbf{r}) - g u_0^3(\mathbf{r}) = V(\mathbf{r}) u_0(\mathbf{r}).$$
 (3)

If we are considering the Gross–Pitaevskii equation (GPE)⁷⁻⁹ for BECs as a particular NLSE, then $\omega \to \mu_0$, where μ_0 is the chemical potential. [The connection between the NLSE and GPE is discussed among other places in Ref. 18.]

The potential that will make $\psi(r,t) = u_0(r) e^{-i\mu_0 t}$ an exact solution of the GPE is given by the (inverse) relation:

$$V(\mathbf{r}) = \mu_0 - gu_0^2(\mathbf{r}) + \frac{\nabla^2 u_0(\mathbf{r})}{u_0(\mathbf{r})}.$$
 (4)

It is, therefore, the task of the experimenter to create such a potential. For the *N*-soliton solutions we are proposing in this paper, the Laplacian term in Eq. (4) is the major contribution to the confining potential. The term related to the density [i.e., $u_0^2(r)$] deepens the

confining potential for the repulsive case g > 0 and causes relative maxima to develop in the attractive case g < 0. It is important to now regard the potential V(r) as so constructed to be *external* and is not varied with respect to $u_0(r)$. Since the potential is now fixed, the conserved energy is given by (here d is the number of spatial dimensions)

$$E_0 = \int d^d x \Big\{ [\nabla u_0(\mathbf{r})]^2 + \frac{g}{2} u_0^4(\mathbf{r}) + V(\mathbf{r}) u_0^2(\mathbf{r}) \Big\}, \tag{5}$$

and the conserved norm which is related to the number of atoms in the BEC (see Ref. 18) is given by

$$M = \int d^{d}x |\psi(\mathbf{r}, t)|^{2} = \int d^{d}x u_{0}^{2}(\mathbf{r}).$$
 (6)

We note that in the attractive case, i.e., g < 0, the development of relative maxima in the potential affects the stability of the solution as we increase the norm M. Soliton wave functions in 1D, 2D, and 3D are discussed in Sec. III.

The linear stability of such solutions in the constructed potential is found by considering a small perturbation of the exact solution Eq. (2), and seeing if this perturbation grows in time. That is, we replace $\psi(\mathbf{r},t)$ with a perturbation series expansion in the small parameter $\varepsilon(\ll 1)$,

$$\widetilde{\psi}(\mathbf{r},t) = \psi_0(\mathbf{r},t) + \varepsilon \, \phi(\mathbf{r},t) + \cdots$$

$$= e^{-i\mu_0 t} \, u_0(\mathbf{r}) + \varepsilon \, \phi(\mathbf{r},t) + \cdots, \tag{7}$$

where μ_0 is the chemical potential and $u_0(\mathbf{r})$ is the particular solution of Eq. (2) whose stability is in question. To first order in ε , $\phi(\mathbf{r},t)$ and $\phi^*(\mathbf{r},t)$ satisfy

$$\begin{pmatrix}
[h(\mathbf{r}) + gu_0^2(\mathbf{r})] & gu_0^2(\mathbf{r}) \\
-gu_0^2(\mathbf{r}) & -[h(\mathbf{r}) + gu_0^2(\mathbf{r})]
\end{pmatrix} \begin{pmatrix} \phi(\mathbf{r}, t) \\ \phi^*(\mathbf{r}, t) \end{pmatrix}$$

$$= i \partial_t \begin{pmatrix} \phi(\mathbf{r}, t) \\ \phi^*(\mathbf{r}, t) \end{pmatrix}, \tag{8}$$

where $h(\mathbf{r})$ is the Hermitian operator,

$$h(\mathbf{r}) = -\nabla^2 + V_0(\mathbf{r}),\tag{9}$$

$$V_0(\mathbf{r}) = V(\mathbf{r}) + gu_0^2(\mathbf{r}) = \mu_0 + \frac{\nabla^2 u_0(\mathbf{r})}{u_0(\mathbf{r})}.$$
 (10)

Solutions to the linear response Eq. (8) are discussed in Sec. IV.

III. MULTI-SOLITON SOLUTIONS

A. One dimension

Let us first choose for our two-trapped soliton wave function, the sum of two Gaussians in 1D. For this case, the solution $u_0(x)$ is given by

$$u_0(x) = A_0 \left[e^{-a(x-q)^2/2} + e^{-a(x+q)^2/2} \right]$$

= $2A_0 e^{-a(q^2 + x^2)/2} \cosh(aqx)$. (11)

The conserved mass follows from Eq. (6) and gives

$$M_0 = \int_{-\infty}^{\infty} \mathrm{d}x \, u_0^2(x) = 2\sqrt{\frac{\pi}{a}} \left(1 + e^{-aq^2}\right) A_0^2,\tag{12}$$

with the respective confining potential [cf. Eq. (4)] given by

$$V(x) = V_0(x) - g u_0^2(x), \tag{13a}$$

$$V_0(x) = \mu_0 + u_0''(x)/u_0(x)$$

$$= a^2 x (x - 2q \tanh(aqx)),$$
(13b)

where we have chosen $\mu_0 = a(1 - aq^2)$ so that $V_0(0) = 0$. [The primes in Eq. (13b) stand for differentiation wrt x.] Plots of the density $\rho_0(x) = u_0^2(x)$ and the confining potential V(x) are shown in the top and bottom panels of Fig. 1 as functions of x with parameter values a = 1, q = 5, and $M_0 = 10$ for $g = \pm 1$. We note that we have set the chemical potential $\mu_0 = -24$ so that V(0) = 0 therein. It can be discerned from the bottom panel of the figure that for this two-soliton ansatz, V(x) consists of two near harmonic wells located at $x = \pm q$ when g = 1. On the other hand, and for g = -1, the potential contains two double-well potentials whose local maxima are located similarly at $x = \pm q$.

The odd two-Gaussian soliton is defined by

$$u_1(x) = A_1 \left[e^{-a(x-q)^2/2} - e^{-a(x+q)^2/2} \right]$$

= $2A_1 e^{-a(q^2+x^2)/2} \sinh(aqx)$,

with conserved mass

$$M_1 = \int_{-\infty}^{\infty} dx u_1^2(x) = 2\sqrt{\frac{\pi}{a}} \left(1 - e^{-aq^2}\right) A_1^2, \tag{14}$$

and confining potential given by

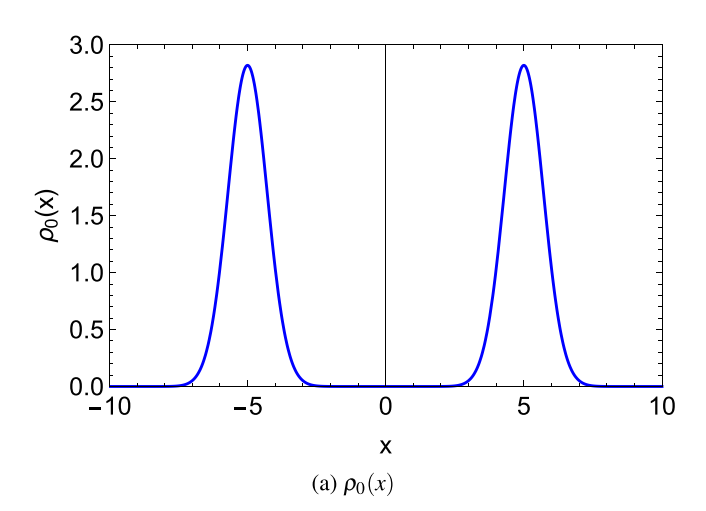
$$V(x) = V_1(x) - g u_1^2(x), (15a)$$

$$V_1(x) = \mu_0 + u_1''(x)/u_1(x)$$

$$= a^2 x \left(x - 2q \coth(aqx) \right), \tag{15b}$$

has nearly the same soliton density distribution for these parameters, and only a slightly different confining potential. Indeed, we compare $V_0(x)$ (even soliton) and $V_1(x)$ (odd soliton) in Fig. 2 [see, also, Eqs. (13b) and (15b)], which showcases that the only difference between them is the behavior near the origin. An experimenter would be hard pressed to construct potentials, which would distinguish between even and odd solitons. Similar results can be obtained by using $\operatorname{sech}[a(q\pm x)]$ functions rather than Gaussian ones to construct two soliton densities.

Stability of these solutions with regard to width stretching can be studied using Derrick's theorem. ¹⁹ This theorem states that if the energy is a minimum under the transformation $x \to \beta x$, i.e., dilation, keeping the mass constant, the soliton is stable. The stretched



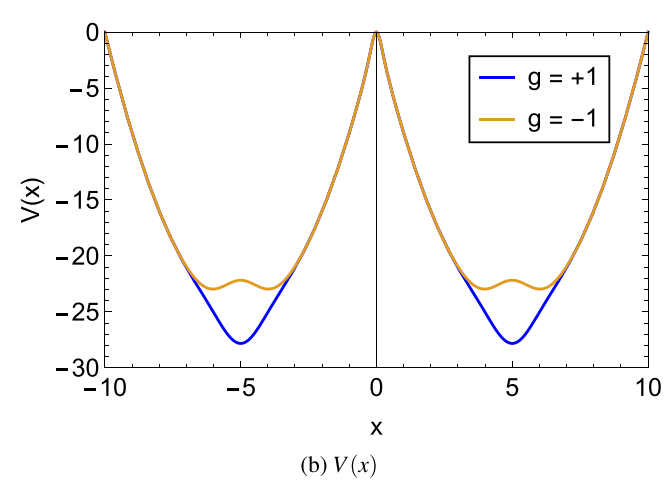


FIG. 1. Plot of the density $\rho_0(x)$ (top) and confining potential V(x) (bottom) both as functions of x for $g=\pm 1$, and for the case when a=1, q=5, and $M_0=10$. The chemical potential is $\mu_0=a(1-aq^2)=-24$. (a) $\rho_0(x)$, (b) V(x).

wave function for the Gaussian case $u_0(x)$ then becomes

$$u_s(x) = 2A_s e^{-a[q^2 + (\beta x)^2]/2} \cosh(aq\beta x),$$
 (16)

where now the mass is given by

$$M_0 = \int_{-\infty}^{\infty} dx u_s^2(x) = \frac{2}{\beta} \sqrt{\frac{\pi}{a}} \left(1 + e^{-aq^2} \right) A_s^2.$$
 (17)

Defining $e_i(\beta) := E_i(\beta)/M_0$, the energy (5) is then the sum of three terms: $e(\beta) = e_1(\beta) + e_2(\beta) + e_3(\beta)$, where

$$e_1(\beta) = \frac{1}{M_0} \int dx \, u_s^{\prime 2}(x) = \frac{a\beta^2}{2} \left[1 - \frac{2aq^2}{1 + e^{aq^2}} \right],$$
 (18a)

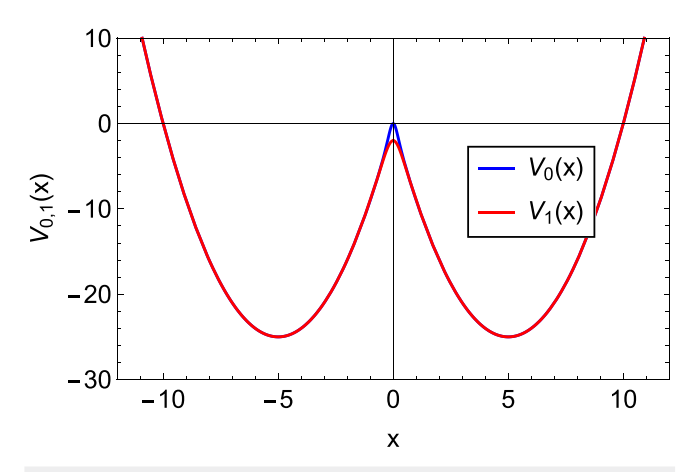


FIG. 2. Plots of $V_0(x)$ and $V_1(x)$ both as functions of x for the even and odd solitons that are given by Eqs. (13b) and (15b), respectively.

$$e_{2}(\beta) = \frac{g}{2M_{0}} \int dx \, u_{s}^{4}(x)$$

$$= \frac{gM_{0} \, \beta \sqrt{a}}{4\sqrt{2\pi}} \frac{(4e^{aq^{2}/2} + e^{2aq^{2}} + 3)}{(1 + e^{aq^{2}})^{2}}, \qquad (18b)$$

$$e_{3}(\beta) = \frac{1}{M_{0}} \int dx \, V(x) \, u_{s}^{2}(x)$$

$$= \frac{1}{M_{0}} \int dx [V_{0}(x) - g \, u_{0}^{2}(x)] \, u_{s}^{2}(x), \qquad (18c)$$

with $V_0(x)$ being given by (13b). We note in passing that unlike the integrals in Eqs. (18a) and (18b) which are evaluated explicitly, the integral in Eq. (18c) must be evaluated numerically. The top and bottom panels of Fig. 3 depict the energy $e(\beta)$ as a function of β for g=1 (top panel) and g=-1 (bottom panel), respectively, with parameter values a=1 and q=5 and for several values of M_0 . It can be discerned from the top panel corresponding to the repulsive case (i.e., g=1) that at $\beta=1$, the soliton is always stable for all values of M_0 , however, for the attractive case (i.e., g=-1), the soliton becomes unstable for $M_0\approx 10$.

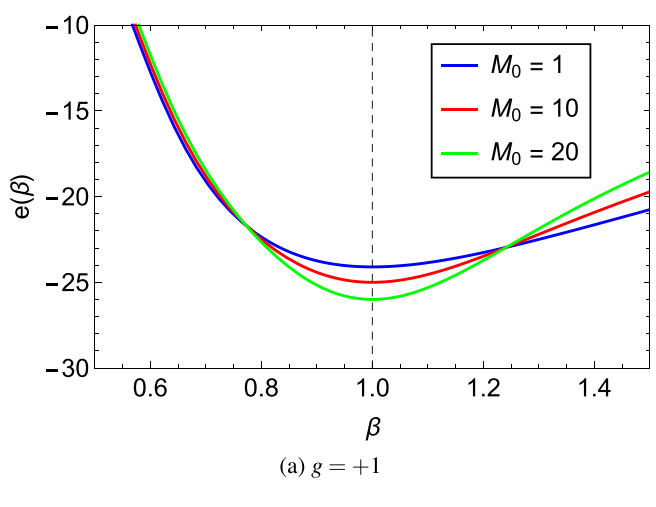
Translational stability can be studied by displacing the soliton solution $u_0(x)$ through the use of the transformation: $x \to x \pm \delta$. In this case, the trial wave function takes the form

$$u_t(x) = A_t \left[e^{-a[x - \delta - q]^2/2} + e^{-a(x + \delta + q)^2/2} \right]$$

= $2A_t e^{-a[(q + \delta)^2 + x^2]/2} \cosh[a(q + \delta)x],$ (19)

where the mass is now given by

$$M_0 = \int_{-\infty}^{\infty} dx \, u_t^2(x) = 2\sqrt{\frac{\pi}{a}} \left(1 + e^{-a(q+\delta)^2}\right) A_t^2.$$
 (20)



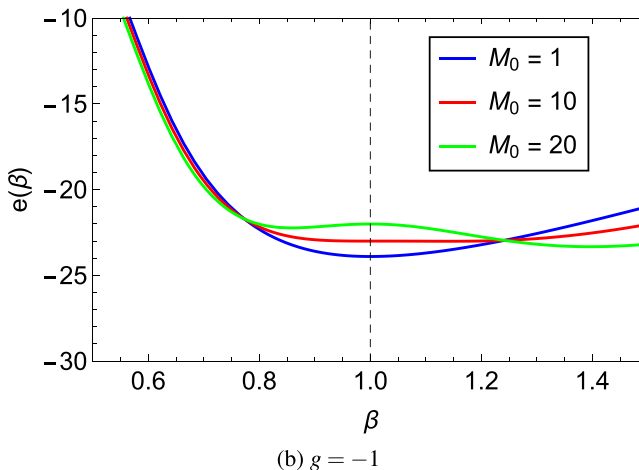


FIG. 3. Plots of energy $e(\beta)$ vs β for $g=\pm 1$ for the case when a=1 and q=5. Note that the soliton for g=1 is always stable whereas for g=-1, it becomes unstable for $M_0\approx 10$. (a) g=+1, (b) g=-1.

Similarly, the energy is the sum of the following terms:

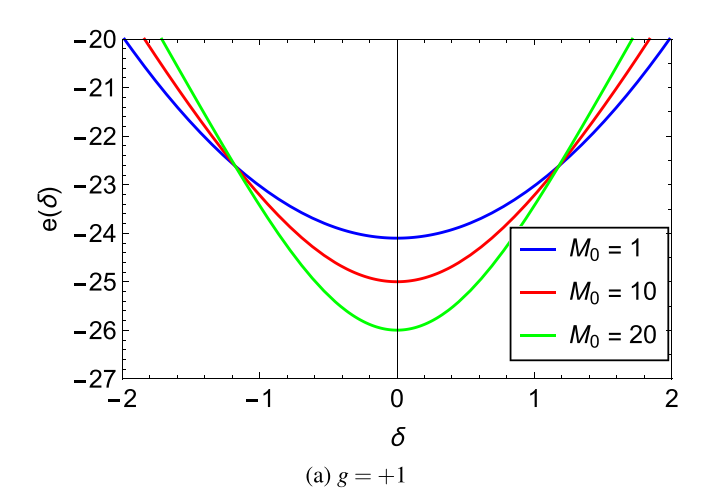
$$e_1(\delta) = \frac{1}{M_0} \int dx \, u_t'^2(x) = \frac{a}{2} \left[1 - \frac{2a(q+\delta)^2}{1 + e^{a(q+\delta)^2}} \right],$$
 (21a)

$$e_2(\delta) = \frac{g}{2M_0} \int dx \, u_t^4(x)$$
$$- gM_0 \sqrt{a} \, (4e^{a(q+\delta)^2/2} + e^{2a(q+\delta)^2} + 3)$$
(21)

$$=\frac{gM_0\sqrt{a}}{4\sqrt{2\pi}}\frac{(4e^{a(q+\delta)^2/2}+e^{2a(q+\delta)^2}+3)}{(1+e^{a(q+\delta)^2})^2},$$
 (21b)

$$e_3(\delta) = \frac{1}{M_0} \int dx \, V(x) \, u_t^2(x)$$

$$= \frac{1}{M_0} \int dx [\, V_0(x) - g \, u_0^2(x) \,] \, u_t^2(x), \tag{21c}$$



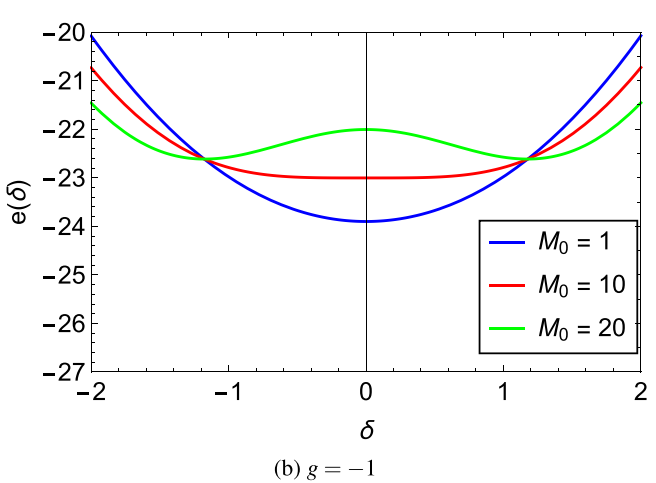


FIG. 4. Same as Fig. 3 but for translational stability. Plots $e(\delta)$ vs δ for g=1 (top panel) and g=-1 (bottom panel) for the cases when a=1 and q=5. Note again that the soliton for g=1 is always stable whereas for g=-1, it becomes unstable for $M_0\approx 10$. (a) g=+1, (b) g=-1.

where $V_0(x)$ is given by (13b). Again, this last integral must be evaluated numerically. We note in passing that the energy components of Eqs. (21a)–(21c) can be respectively, obtained from Eqs. (18a)–(18c) upon setting $\beta=1$ and replacing $q\mapsto q+\delta$. We plot the energy $e(\delta)$ as a function of δ in Fig. 4 for the case with a=1 and q=5, and for several values of M_0 (again, for both g=1 and g=-1). At $\delta=0$, and for the repulsive case (g=1), the soliton is always stable for all values of M_0 , however for the attractive case (g=-1), the soliton again becomes unstable for $M_0\approx 10$.

Based on the above two variational studies, we conclude that most likely the two soliton solutions are always stable for repulsive case (g = 1) but become unstable for the attractive case (g = -1). We have also studied a two-soliton wave function of the form: $u_0(x, y) = A[\operatorname{sech}(q - x) + \operatorname{sech}(q + x)]$, which gives a similar density distribution as the Gaussian case. Numerical results for stretching and translational stability for this ansatz are similar to the

Gaussian case discussed above and indicate stability for the repulsive case and instability for $M \gtrsim 10$ for the attractive case. We will not present those results here.

B. Two dimensions

1. Case 1

We proceed next with the construction of a 2D wave function consisting of two Gaussian functions. In particular, we assume a Gaussian in the x direction centered at $x = \pm q$, and one in the y direction centered at y = 0. The ansatz we consider is given explicitly by

$$u_0(x,y) = A_0 \left\{ e^{-[a(x-q)^2 + by^2]/2} + e^{-[a(x+q)^2 + by^2]/2} \right\}$$
$$= 2A_0 e^{-[a(x^2 + q^2) + by^2]/2} \cosh(aqx). \tag{22}$$

For this case, the conserved mass is given by

$$M_0 = \frac{2\pi}{\sqrt{ah}} (1 + e^{-aq^2}) A_0^2, \tag{23}$$

and the confining potential by

$$V(x,y) = V_0(x,y) - g u_0^2(x,y),$$
(24a)

$$V_0(x,y) = \mu_0 + \left\{ \left[\partial_x^2 + \partial_y^2 \right] u_0(x,y) \right\} / u_0(x,y)$$

= $a^2 x^2 + b^2 y^2 - 2a^2 q x \tanh(aqx),$ (24b)

where we have chosen $\mu_0 = a + b - (aq)^2$ so that $V_0(0,0) = 0$. Plots of the density $\rho_0(x,y) = u_0^2(x,y)$ and the potential $V_0(x,y)$ (both as functions of x and y) for the case when a = b = 1, q = 5, and $M_0 = 10$ are shown in Fig. 5.

To study stability with respect to a stretching of the coordinates $x \to \beta x$ and $y \to \beta y$, we use a trial wave function of the form

$$u_s(x, y) = 2A_s e^{-[a((\beta x)^2 + q^2) + b(\beta y)^2]/2} \cosh(aq\beta x),$$
 (25)

where now the mass is given by

$$M_0 = \int d^2x u_s^2(x, y) = \frac{2\pi}{\theta^2 \sqrt{ah}} (1 + e^{-aq^2}) A_s^2.$$
 (26)

Again computing components of the energy under stretching, we find

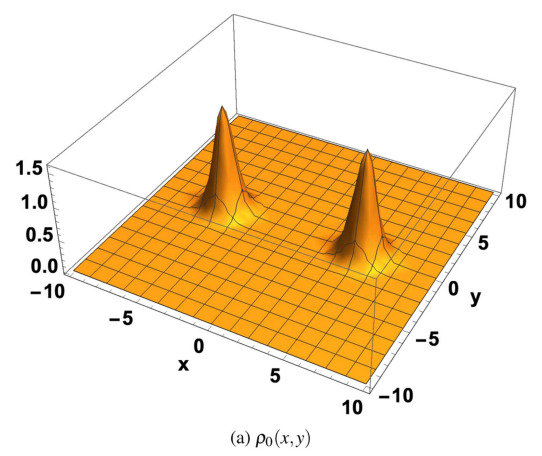
$$e_1(\beta) = \frac{\beta^2}{2} \left[a + b - \frac{2a^2q^2}{1 + e^{aq^2}} \right],$$
 (27a)

$$e_2(\beta) = \frac{gM_0 \,\beta^2 \sqrt{ab}}{16\pi} \, \frac{(8e^{aq^2/2} + 2e^{2aq^2} + 6)}{(1 + e^{aq^2})^2},\tag{27b}$$

$$e_3(\beta) = \frac{1}{M_0} \int d^2x \, V(x, y) \, u_s^2(x, y)$$

$$= \frac{1}{M_0} \int d^2x \left[V_0(x, y) - g \, u_0^2(x, y) \, \right] u_s^2(x, y), \tag{27c}$$

where the integral in Eq. (27c) has to be evaluated numerically. The total energy $e(\beta) = e_1(\beta) + e_2(\beta) + e_3(\beta)$ is presented in Fig. 6 as



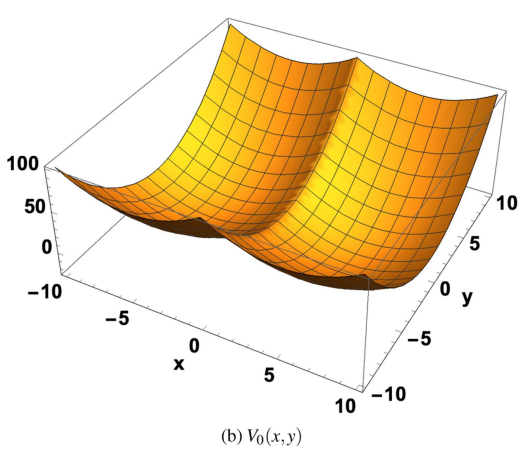


FIG. 5. (a) Plots of the density $\rho_0(x,y)$ and (b) confining potential $V_0(x,y)$ as functions of x and y for the case when a=b=1, q=5, and $M_0=10$. The chemical potential is $\mu_0=b+2{\rm sech}^2(a)-1=0.000\,363$.

a function of β for $g = \pm 1$ for the case when a = b = 1 and q = 5 and for various values of the mass M_0 .

It can be discerned from the figure that at $\beta=1$, the soliton for the repulsive case (i.e., g=1) is always stable for all values of M_0 , whereas for the attractive case (g=-1), the soliton remains stable for values of $M_0 \lesssim 30$ but becomes unstable for larger values of M_0 .

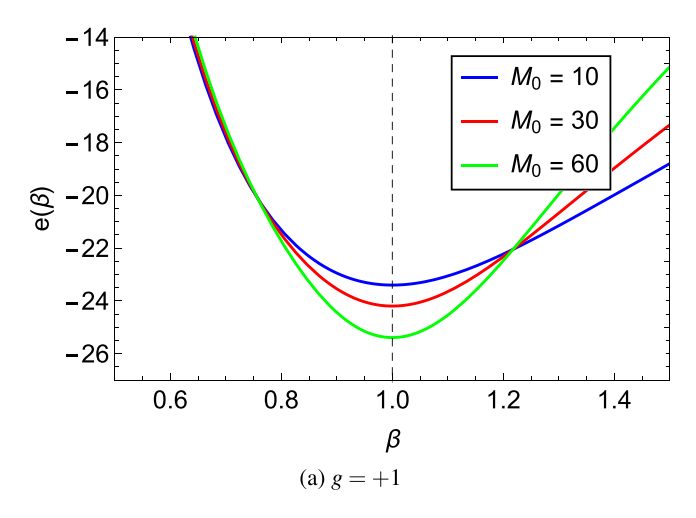
Translational stability is studied by making the replacement $q \to q + \delta$ and computing the energy as a function of δ . The trial wave function in this case is given by

$$u_t(x, y) = 2A_t e^{-[a(x^2 + (q+\delta)^2) + by^2]/2} \cosh[a(q+\delta)x],$$
 (28)

where the total mass reads

$$M_0 = \int d^2x u_t^2(x, y) = \frac{2\pi}{\sqrt{ah}} \left(1 + e^{-a(q+\delta)^2}\right) A_t^2.$$
 (29)

Same as before, the energy terms in this case, i.e., for translational stability are obtained from Eq. (27) by setting $\beta=1$ followed by the replacement $q\mapsto q+\delta$. The results for this case are shown in



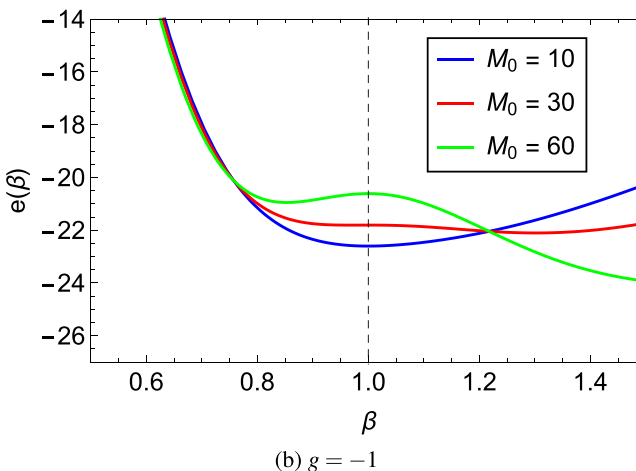


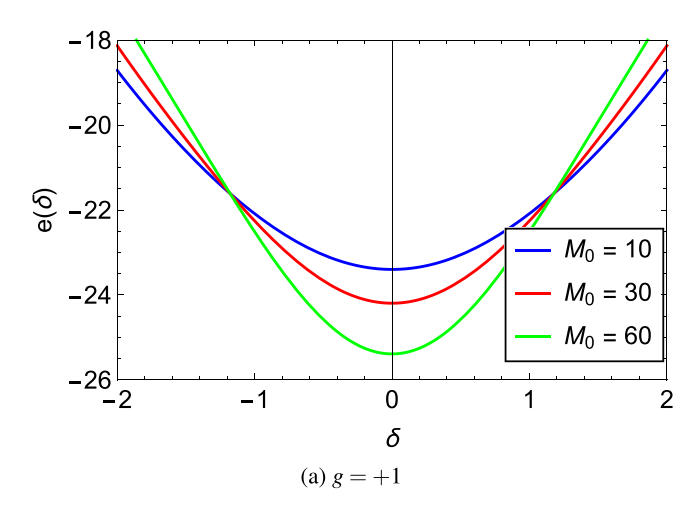
FIG. 6. Plots of the total energy $e(\beta)$ vs β for g=1 (top panel) and g=-1 (bottom panel) and for case 1 when a=b=1 and q=5. (a) g=+1, (b) g=-1.

Fig. 7 where the energy $e(\delta)$ is plotted against δ for g=1 and g=-1 (see the top and bottom panels, respectively). The soliton solutions for g=1 solitons are always stable whereas the ones with g=-1 are stable for values of mass $M_0\lesssim 30$ and become unstable for larger values of the mass, in agreement with the results of Derrick's theorem in Fig. 6.

2. Case 2

In this case, we construct a 2D wave function consisting of two $\operatorname{sech}(x \pm q)$ functions centered at $x = \pm q$, and a Gaussian in the y direction centered at y = 0. Explicitly we choose

$$u_0(x, y) = A_0[\operatorname{sech}(x+q) + \operatorname{sech}(x-q)]e^{-by^2/2}.$$
 (30)



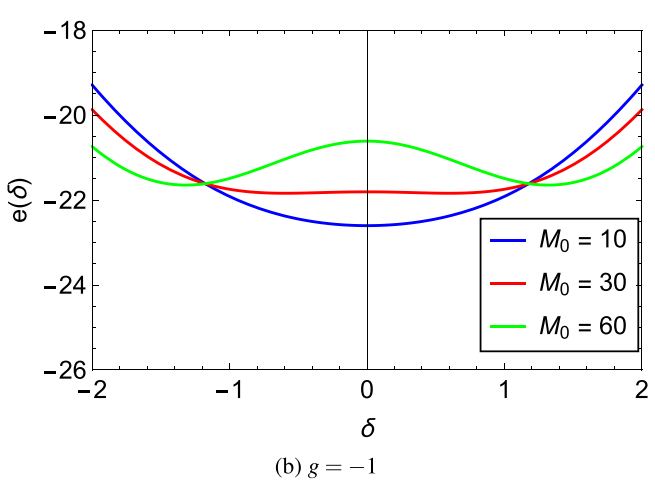


FIG. 7. Same as Fig. 6 but for translational stability. Plots $e(\delta)$ vs δ for g=1 (top panel) and g=-1 (bottom panel) for case 1 when a=b=1 and q=5. (a) g=+1, (b) g=-1.

For this case, the conserved mass is given by

$$M_0 = 4\sqrt{\frac{\pi}{b}} \left[1 + q \operatorname{csch}(q) \operatorname{sech}(q) \right] A_0^2, \tag{31}$$

and the confining potential by

$$V(x,y) = V_0(x,y) - g u_0^2(x,y),$$

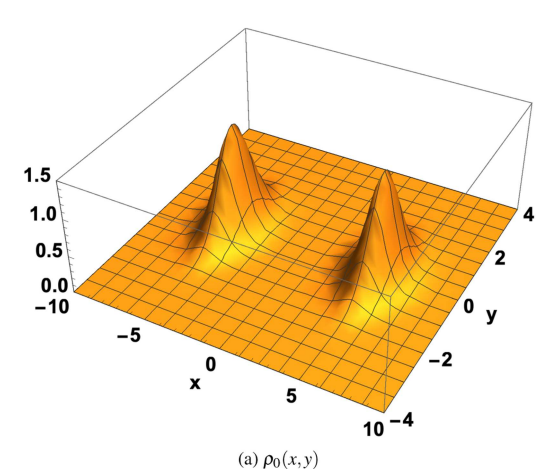
$$V_0(x,y) = \mu_0 + \left\{ \left[\partial_x^2 + \partial_y^2 \right] u_0(x,y) \right\} / u_0(x,y)$$

$$= b^2 y^2 + 2 \operatorname{sech}^2(q) - 2 \left[\operatorname{sech}^2(q-x) - \operatorname{sech}(q-x) \operatorname{sech}(q+x) + \operatorname{sech}^2(q+x) \right],$$
(32b)

where we have chosen $\mu_0 = b + 2 \operatorname{sech}^2(q) - 1$ so that $V_0(0,0) = 0$. Plots of the density $\rho_0(x,y) = u_0^2(x,y)$ and the potential $V_0(x,y)$ as functions of x and y for the case when b = 1, q = 5, and $M_0 = 10$



15 April 2024 19:39:13



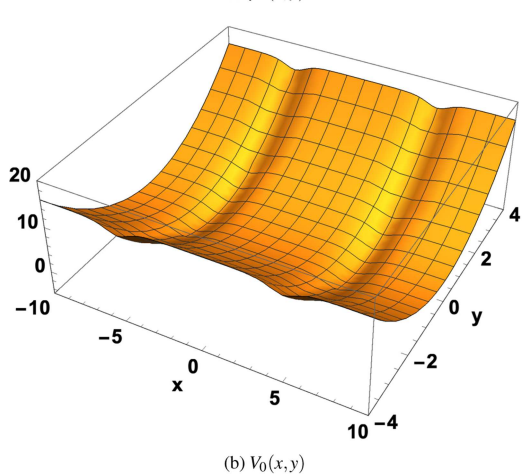


FIG. 8. (a) Plots of the density $\rho_0(x,y)$ and (b) the confining potential $V_0(x,y)$ (again, as functions of x and y) for the case when b=1, q=5, and $M_0=10$. The chemical potential is $\mu_0=b+2{\rm sech}^2(q)-1=0.000\,363$.

are shown in Fig. 8. Note that the trapping potential is quite subtle in shape in the *x* direction and might be difficult to produce experimentally (similar argument applies for the potentials of Figs. 18 and 17, respectively).

The stability with respect to a stretching of the coordinates $x \to \beta x$ and $y \to \beta y$ is carried out by assuming the trial wave function,

$$u_s(x,y) = A_s[\operatorname{sech}(\beta x + q) + \operatorname{sech}(\beta x - q)]e^{-b\beta^2 y^2/2},$$
 (33)

where now the mass is given by

$$M_0 = \frac{4}{\beta^2} \sqrt{\frac{\pi}{b}} [1 + q \operatorname{csch}(q) \operatorname{sech}(q)] A_0^2.$$
 (34)

Upon computing the energy components in this case, we find

$$e_{1}(\beta) = \frac{\beta^{2}}{6[1 + q \operatorname{csch}(q) \operatorname{sech}(q)]} \times \left\{ 2 + 3b + 12 \operatorname{coth}(2q) \operatorname{csch}(2q) - 3q[6 + b + (2 - b) \operatorname{cosh}(4q) \operatorname{csch}^{3}(2q)] \right\}, \qquad (35a)$$

$$e_{2}(\beta) = \frac{gM\beta^{2}}{96} \sqrt{\frac{b}{2\pi}} \frac{\operatorname{csch}(q) \operatorname{sech}(q)}{[2q + \sinh(2q)]^{2}} \times \left\{ -48q + 72q \operatorname{cosh}(2q) - 39 \sinh(2q) + 12 \sinh(4q) + \sinh(6q) \right\}, \qquad (35b)$$

$$e_{3}(\beta) = \frac{1}{M_{0}} \int d^{2}x \, V(x, y) \, u_{s}^{2}(x, y)$$

$$= \frac{1}{M_{0}} \int d^{2}x \, [V_{0}(x, y) - g \, u_{0}^{2}(x, y)] \, u_{s}^{2}(x, y), \qquad (35c)$$

where the integral in Eq. (35c) has to be evaluated numerically. The total energy $e(\beta) = e_1(\beta) + e_2(\beta) + e_3(\beta)$ is presented in Fig. 9 as a function of β for $g = \pm 1$ for the case when a = b = 1 and q = 5 and for various values of the mass M_0 .

It can be discerned from the figure that at $\beta = 1$, the soliton for the repulsive case (i.e., g = 1) is always stable for all values of M_0 , whereas for the attractive case (g = -1), the soliton remains stable for values of $M_0 \lesssim 20$ but becomes unstable for larger values of M_0 .

Translational stability is studied by making the replacement $q \to q + \delta$ and computing the energy as a function of δ . The trial wave function in this case is given by

$$u_t(x, y) = A_t[\operatorname{sech}(x + q + \delta) + \operatorname{sech}(x - q - \delta)]e^{-by^2/2}, \quad (36)$$

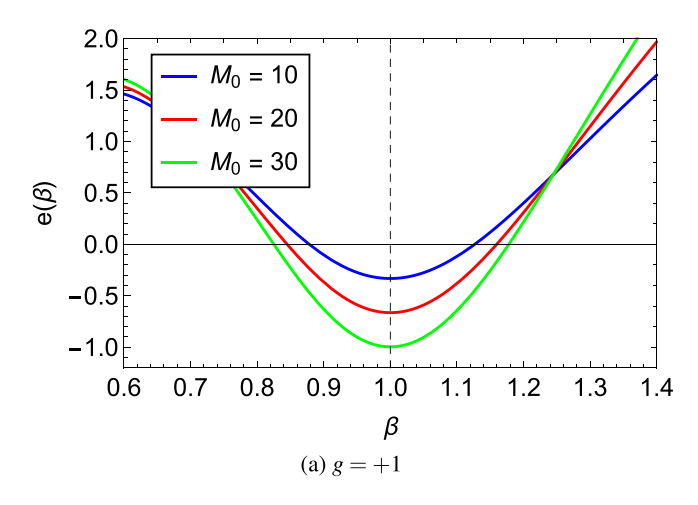
where the total mass is now given by

$$M_0 = 4\sqrt{\frac{\pi}{b}} \left[1 + (q + \delta)\operatorname{csch}(q + \delta)\operatorname{sech}(q + \delta) \right] A_t^2.$$
 (37)

Again, the energy terms for translational instability are obtained from the expressions (35) by setting initially $\beta=1$ and making the replacement $q\to q+\delta$ afterwards. The results in this case for the energy $e(\delta)$ as a function of δ are shown in Fig. 10. The g=1 solitons are always stable whereas the g=-1 solitons are stable for values of mass $M_0\lesssim 20$ and become unstable for larger values of the mass, in agreement with the results of Derrick's theorem in Fig. 9.

C. Three dimensions

Two spheroidal BEC solitons have been studied for a variety of reasons in the literature, the most intriguing being to determine whether modifications of quantum mechanics due to general relativity can be seen in this type of system. In most of these problems, an approximate confining potential is used so that questions of stability of the BEC as one increases the number of atoms can be addressed. Indeed, we can first reverse engineer the exact potential needed to make the sum of two Gaussians an exact solution. Then, we can determine the stability criteria for soliton solutions using Derrick's theorem as well as linear response theory.



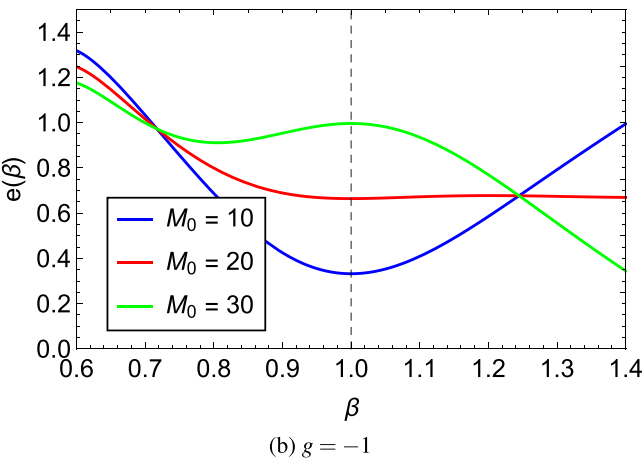


FIG. 9. Plots of the total energy $e(\beta)$ vs β for g=1 (top panel) and g=-1 (bottom panel) and for case 2 when b=1 and q=5. (a) g=+1, (b) g=-1.

1. Two solitons

We start by constructing a 3D Gaussian, two-soliton solution of the form

$$u_0(x, y, z) = A_0 e^{-a(x^2 + y^2)/2} \left[e^{-b(q+z)^2/2} + e^{-b(q-z)^2/2} \right]$$

= $2A_0 e^{-[a(x^2 + y^2) + b(z^2 + q^2)]/2} \cosh(bqz).$ (38)

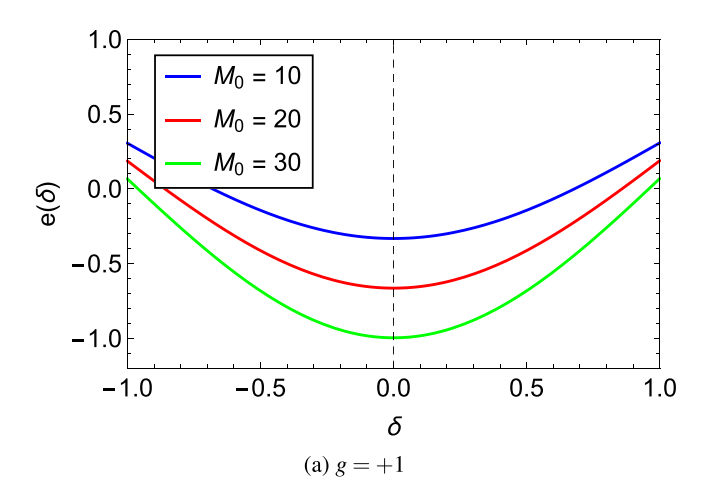
Here, we chose the center of the soliton at x = y = 0 and $z = \pm q$ for simplicity. The mass is now given by

$$M_0 = \frac{2\pi^{3/2}}{a\sqrt{h}} (1 + e^{-bq^2}) A_0^2, \tag{39}$$

and the confining potential by

$$V(x, y, z) = V_0(x, y, z) - g u_0^2(x, y, z),$$

$$V_0(x, y, z) = a^2(x^2 + y^2) + b^2 z^2 - 2b^2 q z \tanh(bqz),$$
(40)



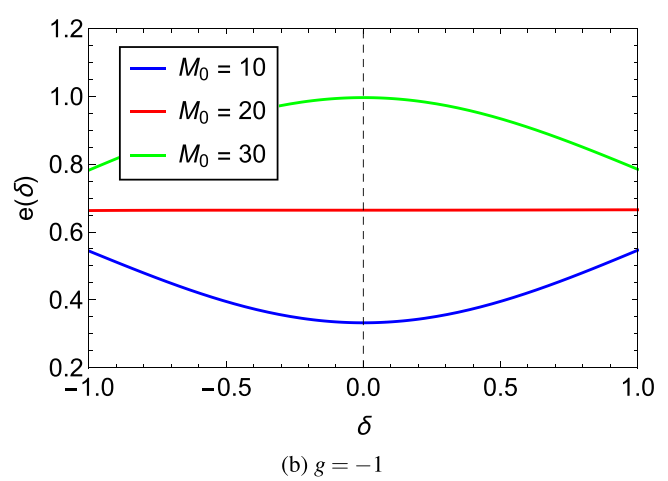


FIG. 10. Same as Fig. 9 but for translational stability. Plots of $e(\delta)$ vs δ for g=1 (top panel) and g=-1 (bottom panel) for case 2 when b=1 and q=5. (a) g=+1, (b) g=-1.

where we have chosen $\mu_0 = b + 2a - b^2q^2$ so that $V_0(0,0,0) = 0$. Plots of the density $\rho_0(x,y,z)$ and potential $V_0(x,y,z)$ as functions of x, y, and z are shown in Fig. 11.

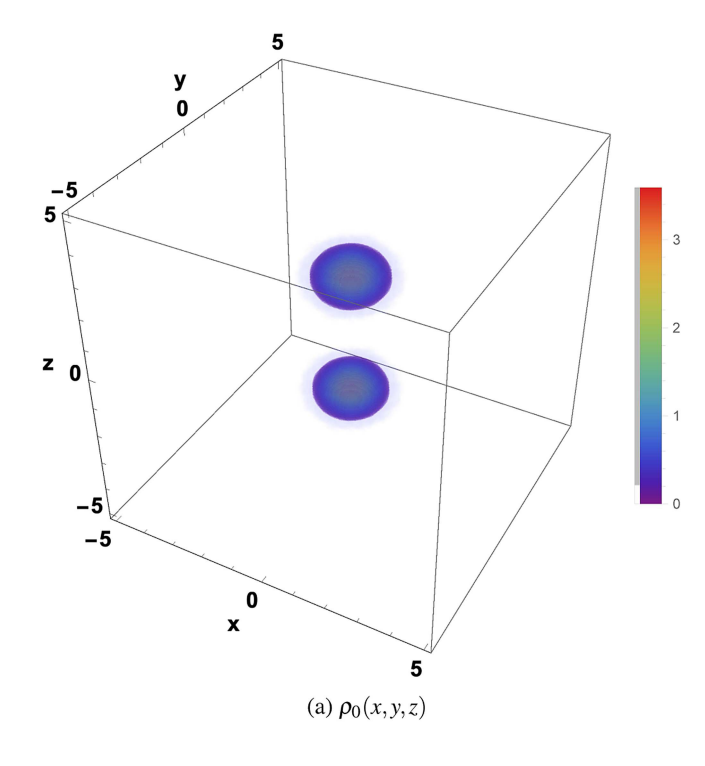
2. Three solitons

There are many possibilities for obtaining N-soliton solutions in 3D. The simplest three soliton case is given by

$$u_0(x, y, z) = A_0 e^{-[a(x^2 + y^2)/2 + bz^2]/2} H_n(\sqrt{b} z),$$
 (41)

where $H_n(\zeta)$ is a Hermite polynomial of order n. In this case, the conserved mass is given by

$$M_0 = \frac{\pi^{3/2} 2^2 n!}{a\sqrt{b}} A_0^2, \tag{42}$$



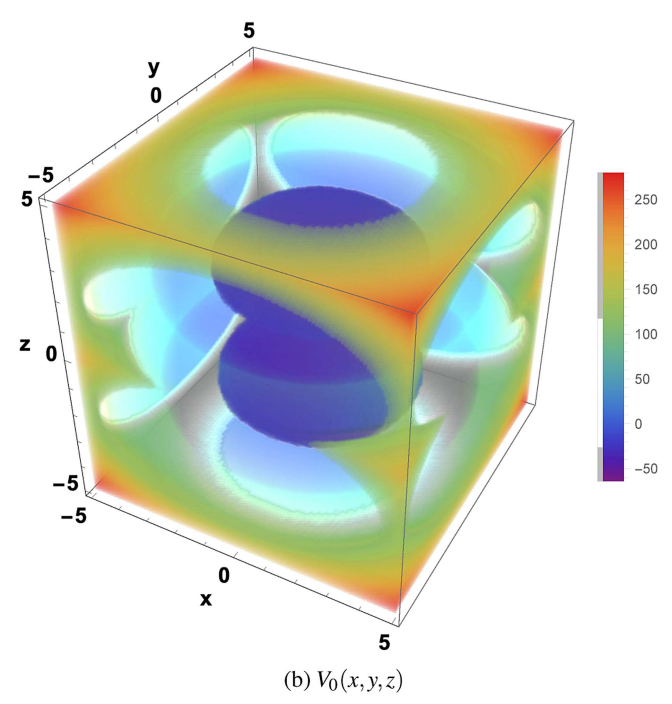


FIG. 11. (a) Plots of the density $\rho_0(x,y,z)$ and (b) the confining potential $V_0(x,y,z)$ (both as functions of x, y, and z) for the case when a=2, b=4, q=2, and $M_0=10$. The chemical potential is $\mu_0=b+2a-(bq)^2=-56$.

and the confining potential by

$$V(x, y, z) = V_0(x, y, z) - g u_0^2(x, y, z),$$

$$V_0(x, y, z) = 2bn + a^2(x^2 + y^2) + b^2 z^2$$
(43)

$$-\frac{4b^{3/2}\,nz\,H_{n-1}(\sqrt{b}\,z)-4b\,n(n-1)\,H_{n-2}(\sqrt{b}\,z)}{H_{n}(\sqrt{b}\,z)}$$

where we have chosen $\mu_0=2a+(2n+1)$ b so that $V_0(0,0,0)=0$. Plots of the density $\rho_0(x,y,z)$ and potential $V_0(x,y,z)$ (both as functions of x,y, and z) are shown in Fig. 12 for the three soliton case with parameter values n=2, a=1, b=2, and $M_0=10$. One can analytically determine the energy of the stretched soliton in this case with $x_i\to\beta x_i$ (i=1,2,3) keeping the mass M fixed. The total energy in this case is

$$e(\beta) = e_1(\beta) + e_2(\beta) + e_3(\beta),$$
 (44)

with

$$e_1(\beta) = \frac{1}{2}\beta^2(2a+5b),$$
 (45a)

$$e_2(\beta) = \frac{41a\sqrt{b}\beta^3 gM}{256\sqrt{2}\pi^{3/2}},\tag{45b}$$

$$e_3(\beta) = \frac{2a + 5b}{2\beta^2}$$

$$-\frac{a\sqrt{b}\left(2\beta^8 - 16\beta^6 + 69\beta^4 - 16\beta^2 - 2\right)\beta^3gM}{4\pi^{3/2}\left(\beta^2 + 1\right)^{11/2}}.$$
 (45c)

One easily verifies that $\beta = 1$ is a stationary point. Setting the second derivative to zero at $\beta = 1$ gives the criterion for instability of the g < 0 soliton to set in, that is,

$$M_c = -g \frac{2048\sqrt{2}\pi^{3/2}(2a+5b)}{1527a\sqrt{b}}. (46)$$

For g = -1, a = 2, b = 2 we find $M_c = 89.62$.

IV. LINEAR RESPONSE EQUATIONS

Solutions of the linear response equations (8) are obtained by consideration of an eigenvalue equation. Let the pair $(a(r), b(r)) \in \mathbb{C}^2$ satisfy the skew-symmetric eigenvalue equation

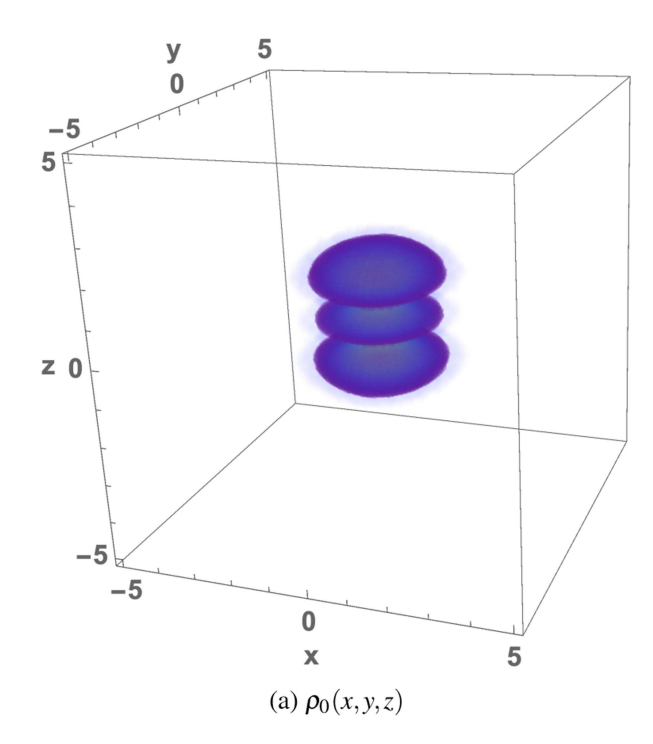
$$\begin{pmatrix} \begin{bmatrix} h(\mathbf{r}) + gu_0^2(\mathbf{r}) \end{bmatrix} & gu_0^2(\mathbf{r}) \\ -gu_0^2(\mathbf{r}) & -\begin{bmatrix} h(\mathbf{r}) + gu_0^2(\mathbf{r}) \end{bmatrix} \end{pmatrix} \begin{pmatrix} a(\mathbf{r}) \\ b(\mathbf{r}) \end{pmatrix} = \lambda \begin{pmatrix} a(\mathbf{r}) \\ b(\mathbf{r}) \end{pmatrix}, (47)$$

where $\lambda = \lambda_r + i\lambda_i \in \mathbb{C}$ is the eigenvalue (or, frequency of oscillations⁹) with λ_r and λ_i representing its real and imaginary parts, respectively. Here, h(r) is given by (9),

$$h(\mathbf{r}) = -\nabla^2 + V_0(\mathbf{r}),\tag{48}$$

and is *independent* of the mass M_0 . Equation (47) is sometimes called the Bogoliubov–de Gennes (BdG) equation.^{20,21}

By taking the complex conjugate of (47), interchanging top and bottom lines, and multiplying by -1, we see that if (a(r), b(r)) is a pair of solutions with eigenvalue λ , then $(b^*(r), a^*(r))$ is a pair of solutions of (47) with eigenvalue $-\lambda^*$. In other words, the eigenvalues come as pairs, λ and $-\lambda^*$. Multiplying the bottom line of (47)



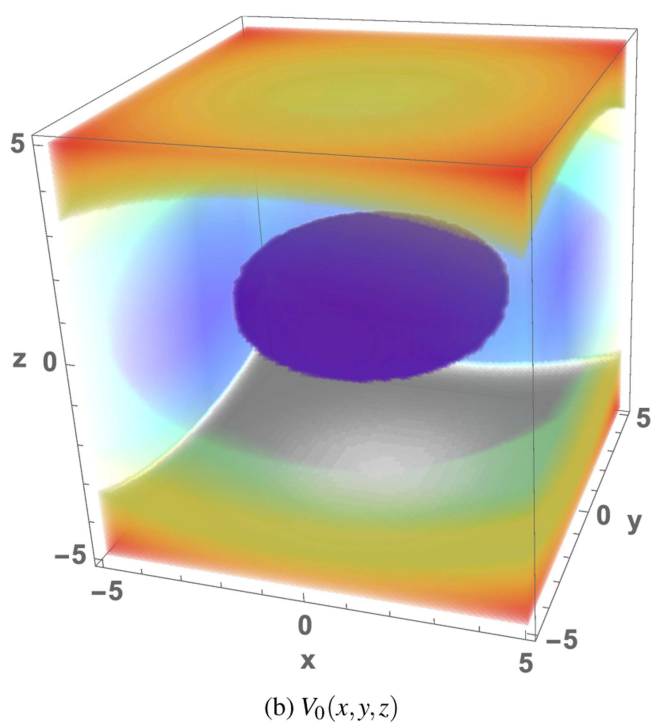


FIG. 12. (a) Plots of the density $\rho_0(x,y,z)$ and (b) the confining potential $V_0(x,y,z)$ (both as functions of x, y, and z) for the three-soliton Hermite case when n=2, a=1, b=2, and $M_0=10$. The chemical potential is $\mu_0=2a+5b=12$.

by -1 and making use of the Hermitian property of the operator on the left-hand-side yields an orthogonality relation

$$(\lambda_l^* - \lambda_m) \int d^3x [a_l^*(\mathbf{r}) a_m(\mathbf{r}) - b_l^*(\mathbf{r}) b_m(\mathbf{r})] = 0.$$
 (49)

The system is deemed stable if $\Im(\lambda_l)=0$ for all l. The presence of a complex eigenvalue with positive imaginary part renders the solution to be unstable. If such an eigenvalue has zero real part, it will correspond to an exponential instability (i.e., exponential growth). The presence of a pure complex eigenvalue in the spectrum would correspond to an oscillatory instability (i.e., oscillations with growing amplitude). For real eigenvalues, the states are normalized by

$$\int d^3x [a_l^*(\mathbf{r})a_m(\mathbf{r}) - b_l^*(\mathbf{r})b_m(\mathbf{r})] = \delta_{l,m}.$$
 (50)

The general solution to (8) is then given by the sum over all eigenstates of (47),

$$\Phi(\mathbf{r},t) = \begin{pmatrix} \phi(\mathbf{r},t) \\ \phi^*(\mathbf{r},t) \end{pmatrix} = \sum_{\text{all}n} \Phi_n \begin{pmatrix} c_n(\mathbf{r}) \\ d_n^*(\mathbf{r}) \end{pmatrix} e^{-i\lambda_n t}
= \sum_{n>0} \Phi_n \left\{ \begin{pmatrix} a_n(\mathbf{r}) \\ b_n(\mathbf{r}) \end{pmatrix} e^{-i\lambda_n t} + \begin{pmatrix} b_n^*(\mathbf{r}) \\ a_n^*(\mathbf{r}) \end{pmatrix} e^{+i\lambda_n^* t} \right\},$$
(51)

the last sum now going over the unique eigenvalues only. At t = 0,

$$\begin{pmatrix} \phi(\mathbf{r},0) \\ \phi^*(\mathbf{r},0) \end{pmatrix} = \sum_{n} \Phi_n \begin{pmatrix} c_i(\mathbf{r}) \\ d_i^*(\mathbf{r}) \end{pmatrix}. \tag{52}$$

Inverting this relation using (50)

$$\int d^3x \left(c_m^*(\mathbf{r}), d_m(\mathbf{r})\right) \begin{pmatrix} 1 & 0 \\ 0 & -1 \end{pmatrix} \begin{pmatrix} \phi(\mathbf{r}, 0) \\ \phi^*(\mathbf{r}, 0) \end{pmatrix}$$

$$= \sum_{l} \Phi_l \left(c_m^*(\mathbf{r}), d_m(\mathbf{r})\right) \begin{pmatrix} 1 & 0 \\ 0 & -1 \end{pmatrix} \begin{pmatrix} c_l(\mathbf{r}) \\ d_l^*(\mathbf{r}) \end{pmatrix} = \Phi_m \qquad (53)$$

gives

$$\Phi_l = \int d^3x [c_l^*(\mathbf{r})\phi(\mathbf{r},0) - d_l(\mathbf{r})\phi^*(\mathbf{r},0)].$$
 (54)

Solutions of the NLSE to first order are then given by

$$\widetilde{\Psi}(\mathbf{r},t) = \Psi_0(\mathbf{r},t) + \varepsilon \,\Phi(\mathbf{r},t) + \cdots \tag{55}$$

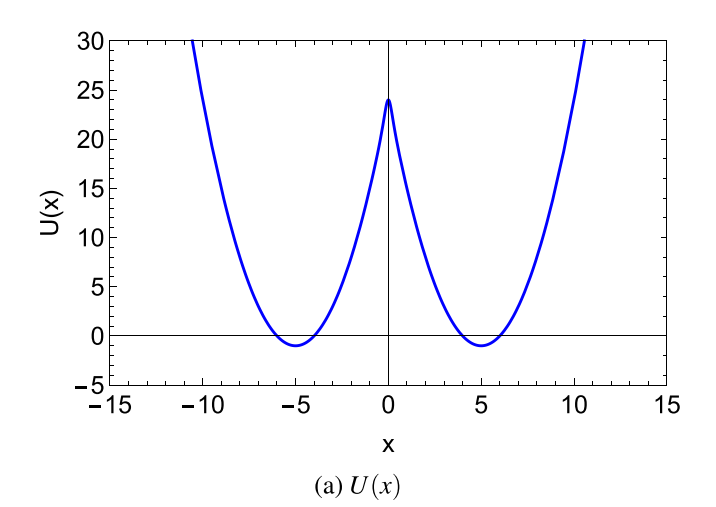
where

$$\Psi_0(\mathbf{r}, t) = \begin{pmatrix} u_0(\mathbf{r}) e^{-i\mu_0 t} \\ u_0(\mathbf{r}) e^{+i\mu_0 t} \end{pmatrix}.$$
 (56)

We must also require that

$$\Psi_0^{\dagger}(\mathbf{r},t) M \Phi(\mathbf{r},t) = 0, \quad M = \begin{pmatrix} 1 & 0 \\ 0 & -1 \end{pmatrix},$$
 (57)

since the unperturbed state is included in $\Psi_0(r,t)$. This requirement is usually applied by omitting the n=0 state in the sum appearing in Eq. (51), as discussed in Sec. IV A 1.



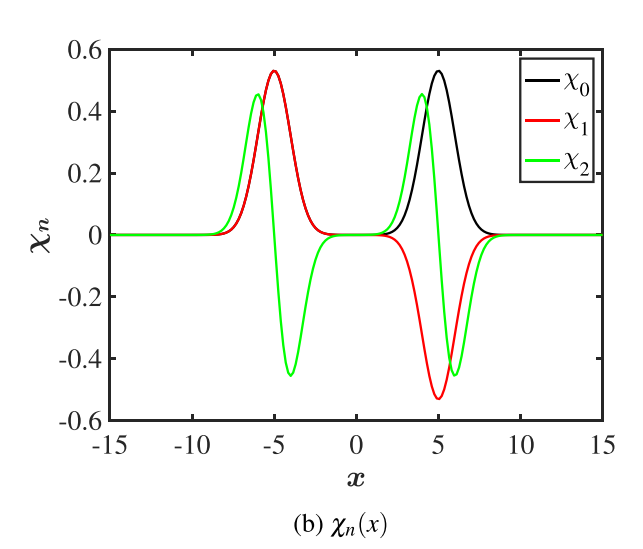


FIG. 13. (a) Plots of the potential U(x) in Eq. (62) and (b) the wave functions $\chi_n(x)$ in Eq. (64) as functions of x for the case when a=1 and q=5.

A. One dimension

In 1D, the eigenvalue equation (47) becomes

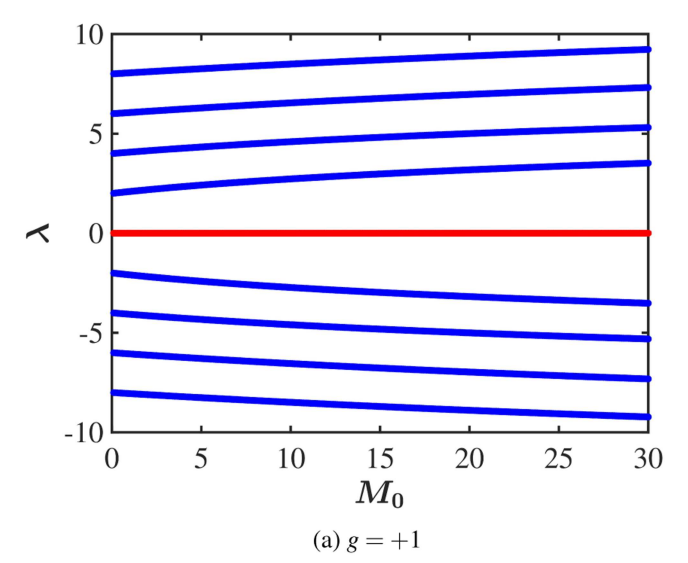
$$\begin{pmatrix}
[h(x) + gu_0^2(x)] & gu_0^2(x) \\
-gu_0^2(x) & -[h(x) + gu_0^2(x)]
\end{pmatrix}
\begin{pmatrix}
a(x) \\
b(x)
\end{pmatrix} = \lambda \begin{pmatrix}
a(x) \\
b(x)
\end{pmatrix},$$
(58)

where $u_0(x)$ is given by Eq. (11), and

$$h(x) = -\partial_x^2 + U(x), \tag{59}$$

$$U(x) = -a(1 - aq^2) + a^2x (x - 2q \tanh(aqx)).$$
 (60)

Here, we have set $\mu = \mu_0 + \lambda$ and defined a potential U(x) so that now $U(0) = \mu_0 = a(1 - aq^2)$. A plot of this potential as a function of x is shown in Fig. 13 for the case when a = 1 and q = 5. Zero



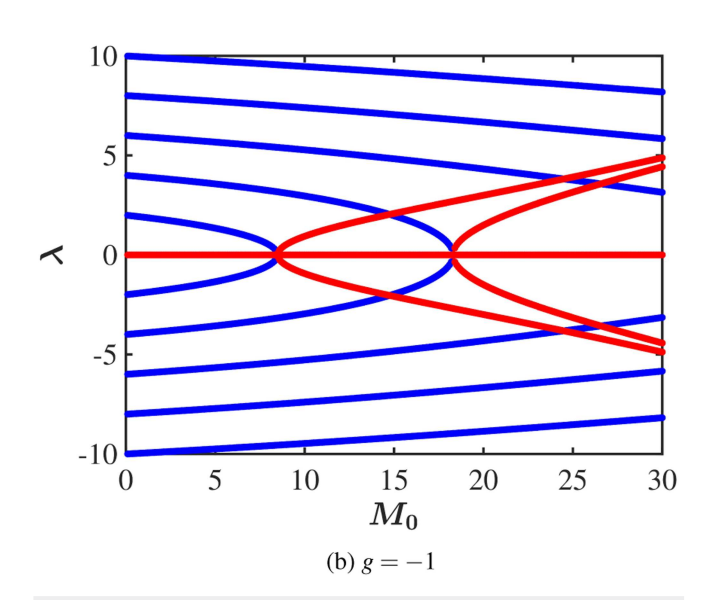


FIG. 14. Real (in blue) and imaginary (in red) parts of the eigenvalues λ in Eq. (58) as functions of M_0 for the one-dimensional case with a=1 and q=5.

eigenvalues ($\lambda = 0$) now correspond to the soliton solution $a(x) = -b(x) = u_0(x)$.

1. Bogoliubov approximation

Moreover, the eigenvalue problem (58) can be written in terms of eigenvectors of the Hermitian operator h(x) in 1D. To that effect, we define

$$h(x) \chi_n(x) = \epsilon_n \chi_n(x), \quad \chi_n(x) \in \mathbb{R},$$
 (61)

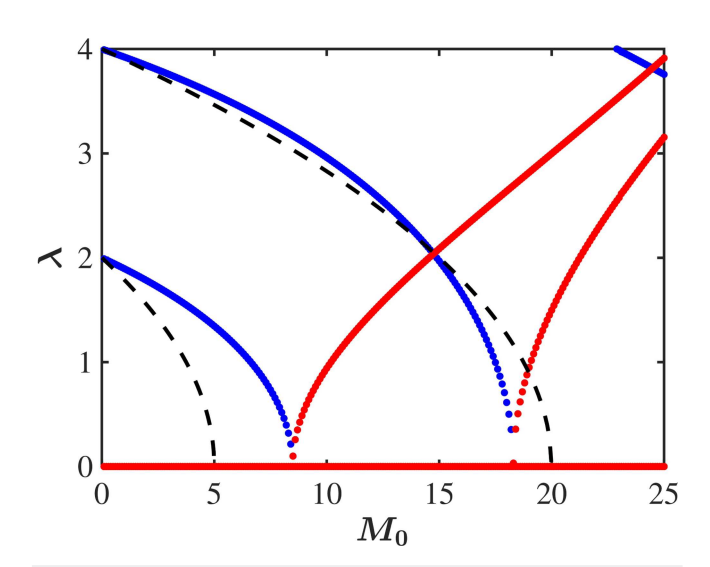


FIG. 15. Comparison of the real part of the g=-1 numerically (exact) eigenvalues λ (in blue) with the Bogoliubov formula (in dashed black) of Eq. (68). The red lines correspond to the imaginary part of λ .

where $\epsilon_n \in \mathbb{R}$ and $\chi_n(x)$ obey the orthonormality relation

$$\int \mathrm{d}x \chi_n(x) \chi_{n'}(x) = \begin{cases} \delta_{n,n'}, & \text{for } n \text{ and } n' \neq 0, \\ M_0, & \text{for } n = n' = 0. \end{cases}$$
 (62)

For our case when a=1 and q=5, the eigenvalues are very close to being doubly degenerate and are given by $\epsilon_n=0,2,4,6,\ldots$ with a small splitting of each state due to tunneling between the two wells. The low-lying spectrum is that of a quantum harmonic oscillator with frequency $\omega=2$, as might be expected from the shape of the double well. A plot of the first few wave functions $\chi_n(x)$ (as functions of x) is shown in Fig. 13. Note that the zero eigenvalue $\lambda=0$ corresponds to the translational mode $a(x)=-b(x)=u_0(x)$.

Expanding the solutions of (58) by setting

$$\begin{pmatrix} a(x) \\ b(x) \end{pmatrix} = \sum_{n=0}^{\infty} \begin{pmatrix} A_n(x) \\ B_n(x) \end{pmatrix} \chi_n(x), \tag{63}$$

and using the orthonormality condition, we obtain the eigenvalue problem

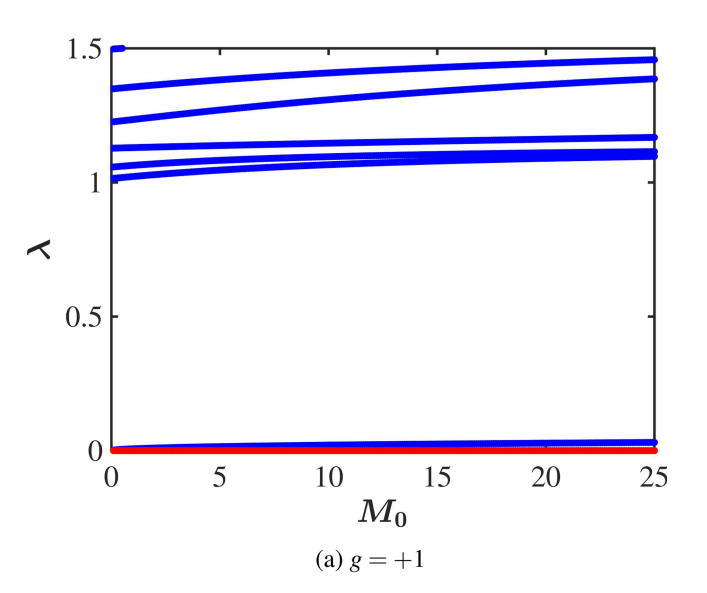
$$\sum_{n'=0}^{\infty} \begin{pmatrix} (\epsilon_n - \lambda)\delta_{n,n'} + g\Delta_{n,n'} & g\Delta_{n,n'} \\ -g\Delta_{n,n'} & -(\epsilon_n + \lambda)\delta_{n,n'} - g\Delta_{n,n'} \end{pmatrix} \times \begin{pmatrix} A_{n'}(x) \\ B_{n'}(x) \end{pmatrix} = 0, \tag{64}$$

where

$$\Delta_{n,n'} = \int dx u_0^2(x) \, u_n(x) u_{n'}(x). \tag{65}$$

The eigenvalues λ are then found by solving the determinant,

$$\begin{vmatrix} (\epsilon_n - \lambda)\delta_{n,n'} + g\Delta_{n,n'} & g\Delta_{n,n'} \\ -g\Delta_{n,n'} & -(\epsilon_n + \lambda)\delta_{n,n'} - g\Delta_{n,n'} \end{vmatrix} = 0.$$
 (66)



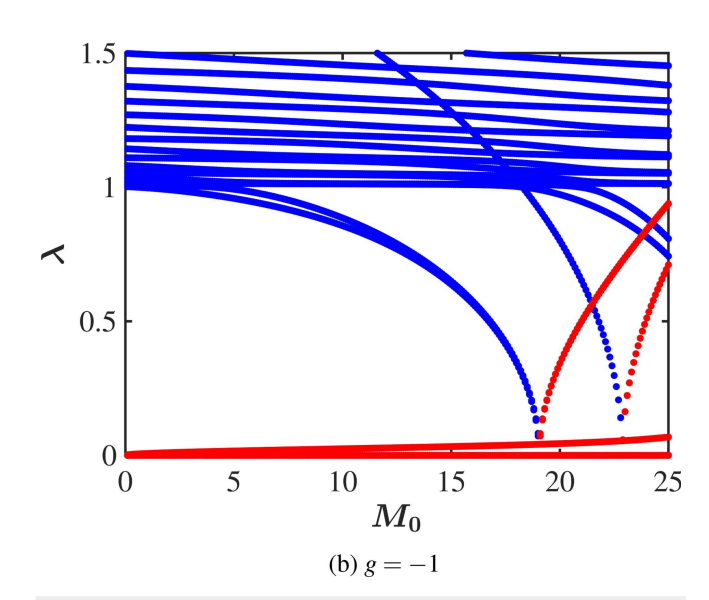


FIG. 16. The real part (in blue) and imaginary part (in red) of the eigenvalues for the two-dimensional soliton of Eq. (30) as functions of M_0 for the $g=\pm 1$ cases, with a=b=1 and q=5. (a) g=+1, (b) g=-1.

Numerical calculations for the case when a=1 and q=5 give $\Delta_{1,1}\approx 0.2\,M_0$ and $\Delta_{2,2}\approx 0.1\,M_0$, whereas $\Delta_{1,2}=10^{-9}\,M_0$ and $\Delta_{0,3}=-0.705\,M_0$. So a reasonable approximation for the low-lying eigenvalues is to include only diagonal terms, $\Delta_{n,n'}\approx \Delta_n\,\delta_{n,n'}$, in which case (66) becomes

$$\begin{vmatrix} \epsilon_n - \lambda + g\Delta_n & g\Delta_n \\ -g\Delta_n & -\epsilon_n - \lambda - g\Delta_n \end{vmatrix} = 0, \tag{67}$$

which gives

$$\lambda_n = \pm \sqrt{\epsilon_n(\epsilon_n + 2g\Delta_n)},\tag{68}$$

which is the Bogoliubov spectrum. One can see here that for g=+1 the system is always stable whereas for g=-1 there is a small region of stability as long as

$$\epsilon_n \ge 2g\Delta_n,$$
 (69)

for any n. For n = 1 in our case, this means that $2 > 0.4 M_0$, or $M_0 < 5$. For n = 2, we find $M_0 < 20$, which is a higher bound.

2. Direct solution of the BdG equation

The eigenvalue equation of Eq. (58) is solved numerically in MATLAB by employing a computational grid in coordinate space and using a fourth-order accurate, finite difference approximation for the Laplacian operator. We corroborated our numerical results by using P_3 finite elements in the computational software FreeFEM++ 24 that utilizes the ARPACK eigenvalue solver 25 and obtained similar results.

In 1D, numerical results for the eigenvalues λ of this calculation are plotted in Fig. 14 as functions of M_0 for $g=\pm 1$ and parameter values a=1 and q=5. The real part of the eigenvalues is shown in blue whereas their imaginary part is shown in red. The top panel of the figure corresponding to the repulsive (g=1) case suggests that the solution is linearly stable. On the other hand, when we consider attractive interactions, i.e., g=-1, the solution is (linearly) stable but becomes unstable past $M_0\gtrsim 8$, in approximate agreement with the Bogoliubov approximation and Derrick's theorem (see Sec. III A). At $M_0=0$, the low-lying eigenvalues are all real and given by $\lambda_n\approx 0,2,4,6,\ldots$

Moreover, we compare the 1D numerical results of Eq. (58) for g = -1 (see the bottom panel of Fig. 14) with the approximate Bogoliubov result from Eq. (68) in Fig. 15. The shape of the Bogoliubov curve shown with a dashed black line is proximal to the numerically computed eigenvalues although the point in the parameter space where the solution is predicted to be unstable is at lower values of M_0 . This is somewhat expected because not enough terms were included in Eq. (66), which itself would allow otherwise a better agreement between the two approaches.

Similar conclusions are drawn in the 2D case (see Sec. III B). To that end, we briefly discuss our findings in Fig. 16, which depicts numerical results for the eigenvalues λ (see also Sec. III B) when a=b=1 and q=5. Again, the system is stable when g=-1 for all values of M_0 , whereas when g=+1 there is a region of stability for $M_0\lesssim 7.5$. We note in passing that we have checked the stability and instability (over the respective parameter regime) of the solutions that we have presented so far by performing direct numerical simulations of the GPE [cf. Eq. (1)] although we omit the presentation of the respective results herein.

V. CONCLUSIONS

In this paper, we considered the Gross–Pitaevskii equation (GPE) also known as the nonlinear Schrödinger equation (NLSE) and employed the "inverse problem" method for determining confining potentials that will support particular confined *N*-soliton solutions. We discussed several such external confining potentials that one obtains by assuming various wave functions for the solution. The solutions to the GPE (NLSE) that we studied possessed an arbitrary number of "soliton-like" maxima, i.e., *N*-soliton solutions.

These solutions were always linearly stable when the self-interaction was repulsive. The use of analytic methods, i.e., Derrick's theorem allowed us to obtain analytic estimates in the attractive setting for the values of the L^2 norm of the solution or, equivalently, the number of atoms in the trap above which these solutions are unstable to width perturbations. We further solved numerically the underlying eigenvalue (Bogoliubov-de Gennes or BdG) problem emanating from the linearization of the GPE whose results are in line (in terms of stability characteristics) with the theoretical predictions from Derrick's theorem. However, in all cases that we have studied in this work that turned out to be unstable (i.e., attractive interactions), the BdG analysis gives a lower value for the critical value of the norm of the wave function than Derrick's theorem or the translational instability. To the extent that we can identify these distinct entities as separate BEC solutions of the GPE, we have given a prescription for what external confining potentials will allow various configurations of BECs that are stable in 1D and higher spatial dimensions.

ACKNOWLEDGMENTS

The motivation for working on this problem resulted from discussions that F.C. had with Alan Chodos on using BECs to test modifications of gravity. F.C., J.F.D., and E.G.C. would like to thank the Santa Fe Institute and the Center for Nonlinear Studies at Los Alamos National Laboratory for their kind hospitality. A.K. is grateful to Indian National Science Academy (INSA) for the award of INSA Honorary Scientist position at Savitribai Phule Pune University. The work of EGC has been supported by the U.S. National Science Foundation under Grant No. DMS-2204782. The work at Los Alamos National Laboratory was carried out under the auspices of the U.S. DOE and under Contract No. DEAC52-06NA25396.

AUTHOR DECLARATIONS

Conflict of Interest

The authors have no conflicts to disclose.

Author Contributions

Fred Cooper: Conceptualization (equal); Formal analysis (equal); Investigation (equal); Methodology (equal); Project administration (equal); Supervision (equal); Validation (equal); Visualization (equal); Writing - original draft (equal); Writing - review & editing (equal). **Avinash Khare:** Conceptualization (equal); Formal analysis (equal); Investigation (equal); Methodology (equal); Supervision (equal); Validation (equal); Visualization (equal); Writing - original draft (equal); Writing - review & editing (equal). John F. Dawson: Conceptualization (equal); Formal analysis (equal); Investigation (equal); Methodology (equal); Project administration (equal); Software (equal); Supervision (equal); Validation (equal); Visualization (equal); Writing - original draft (equal); Writing - review & editing (equal). **Efstathios G. Charalampidis:** Formal analysis (equal); Software (equal); Validation (equal); Visualization (equal); Writing - original draft (equal); Writing - review & editing (equal). Avadh Saxena: Conceptualization (equal); Formal analysis (equal); Investigation (equal); Methodology (equal); Project administration (equal); Supervision (equal); Validation (equal); Writing - original draft (equal); Writing - review & editing (equal).

DATA AVAILABILITY

The data that support the findings of this study are available from the corresponding author upon reasonable request.

APPENDIX: SOME OTHER N-SOLITON SOLUTIONS IN 2D

It is clear that there are infinite possibilities for exact N-soliton solutions in 2D and 3D. Here, we will give two examples not included in the main text. For the sum of Gaussians, it is easy to generalize to N soliton exact solutions. As an example of this, consider the case where the solitons are centered at the ends of an equilateral triangle. That is, we take for the initial condition,

$$u(x,y) = A \left\{ e^{-a(y-\sqrt{3}q)^2/2 - ax^2/2} + e^{-ay^2/2} \left[e^{-a(x-q)^2/2} + e^{-a(q+x)^2/2} \right] \right\},$$
 (A1)

and obtain from the inverse method,

$$\mu_0 = 2a - a^2 q^2 - \frac{a^2 q^2}{e^{aq^2} + 1/2},$$
 (A2)

together with $V(x, y) = V_1(x, y) + V_2(x, y)$ where

$$V_1(x,y) = -A^2 g e^{-a(3q^2 + 2qx + x^2 + y^2)}$$

$$\times \left[e^{aq^2} + e^{aq(x + \sqrt{3}y)} + e^{aq(q + 2x)} \right]^2, \quad (A3)$$

and

$$V_{2}(x,y) = \frac{a^{2}}{\left(2e^{aq^{2}} + 1\right)\left(e^{aq^{2}} + e^{aq(x+\sqrt{3}y)} + e^{aq(q+2x)}\right)}$$

$$\times \left\{e^{aq(q+2x)}\left(-2q^{2} - 2qx + x^{2} + y^{2}\right) + 2e^{2aq^{2}}\left(2qx + x^{2} + y^{2}\right) + e^{aq^{2}}\left(-2q^{2} + 2qx + x^{2} + y^{2}\right) + 2\left(2q^{2} - 2\sqrt{3}qy + x^{2} + y^{2}\right)e^{aq(q+x+\sqrt{3}y)} + 2e^{2aq(q+x)}\left(-2qx + x^{2} + y^{2}\right) + \left(-2\sqrt{3}qy + x^{2} + y^{2}\right)e^{aq(x+\sqrt{3}y)}\right\}.$$
(A4)

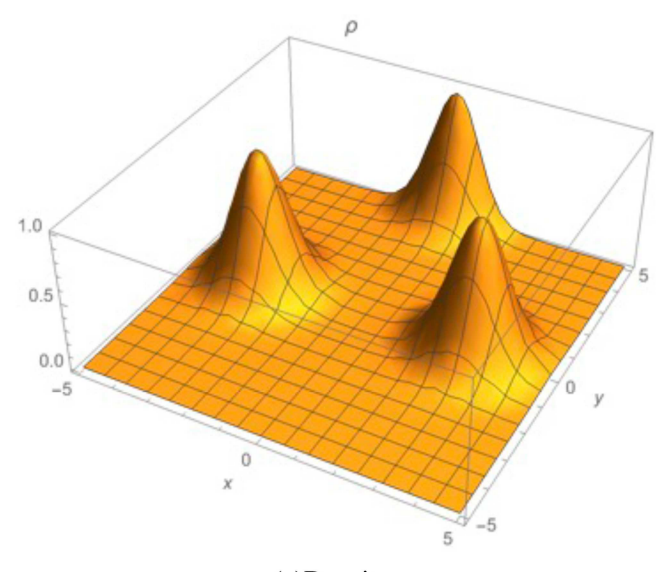
For the choice of parameter values g = -1, A = 1, a = 1, and q = 3, we depict the density $\rho(x, y)$ and potential V(x, y) in Fig. 17.

One can also have solitons along both the x- and y-axes by choosing

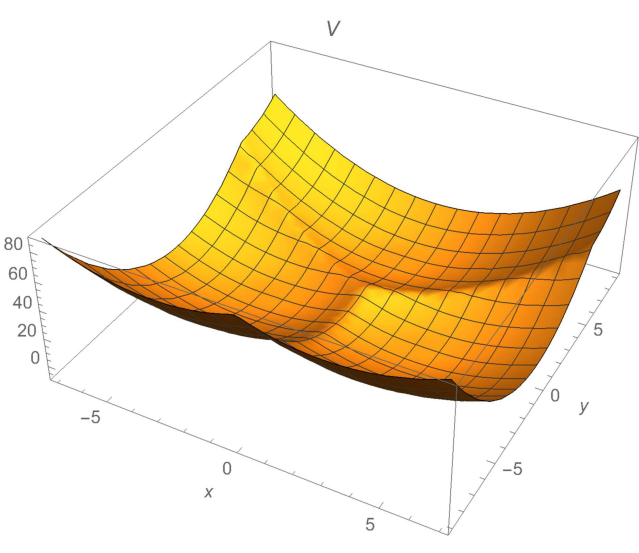
$$u_0(x, y) = AH_n(\sqrt{ax}) H_m(\sqrt{by}) e^{-ax^2/2 - by^2/2},$$
 (A5)

for which one has n + 1 solitons in x-direction and m + 1 solitons in y-direction where

$$V(x,y) = a^{2}x^{2} + b^{2}y^{2}$$
$$-gA^{2} H_{n}^{2}(\sqrt{a}x) H_{m}^{2}(\sqrt{b}y)e^{-ax^{2}/2 - by^{2}/2},$$
(A6)



(a)Density



(b)Confining potential

FIG. 17. The density ρ (x, y) and the confining potential V(x,y) both as functions of x and y for the three soliton case, when g=-1, a=1, q=3, and A=1.

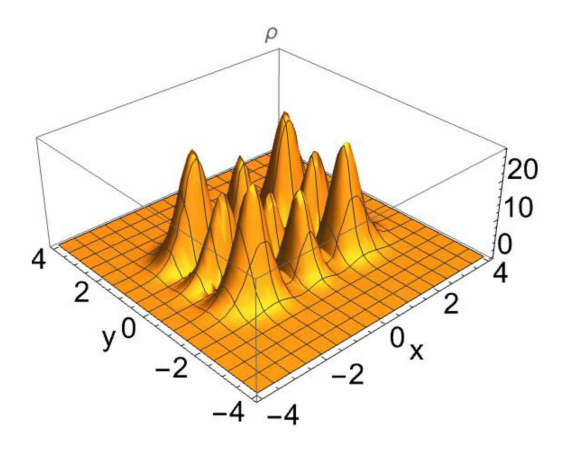
with $\mu_0 = (2n+1)a + (2m+1)b$. When m = n = 2, the trapped solution has nine peaks. For that case, we obtain

$$M_0 = 64\pi A^2 / \sqrt{ab},\tag{A7a}$$

$$\rho(x,y) = A^{2}(2 - 4ax^{2})^{2}(2 - 4by^{2})^{2}e^{-ax^{2} - by^{2}},$$
(A7b)

$$V(x,y) = a^2x^2 + b^2y^2$$

$$-16 A^{2} g (1-2ax^{2})^{2} (1-2by^{2})^{2} e^{-ax^{2}-by^{2}}, \qquad (A7c)$$



(a)Density

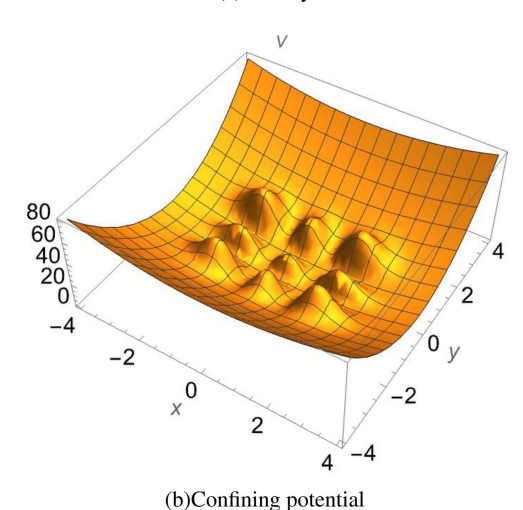


FIG. 18. The density $\rho(x, y)$ and the confining potential V(x, y) both as functions of x and y, for the nine soliton case, when m = n = 2 and g = -1, A = 1, a = 1, and b = 2.

and with $\mu_0 = 5(a + b)$. An example of this for m = n = 2 and A = 1, a = 1, b = 2, and with g = -1 is shown in Fig. 18.

Derrick's theorem in this case allows us to determine the critical mass for instability, which is given by

$$M_c = \frac{81\,920\,\pi(a+b)}{11\,029\sqrt{ab}}.\tag{A8}$$

For a = 1, b = 2, and g = -1, we find

$$M_c = \frac{122\,880\,\sqrt{2}\pi}{11\,029} \approx 49.5.$$
 (A9)

REFERENCES

¹M. J. Ablowitz, B. Prinary, and A. Trubatch, Discrete and Continuous Nonlinear Schrödinger Systems, Vol. 302 (Cambridge University Press, Cambridge, 2004).

²A. Hasegawa and K. Kodama, Solitons in Optical Communications (Clarendon Press, 1995).

³Y. Kivshar and G. Agrawal, Optical Solitons: From Fibers to Photonic Crystals

(Academic Press, 2003). ⁴V. Zakharov, "Stability of periodic waves of finite amplitude on the surface of a deep fluid," J. Appl. Mech. Tech. Phys. 9, 190-194 (1968).

⁵M. J. Ablowitz, Nonlinear Dispersive Waves: Asymptotic Analysis and Solitons (Cambridge University Press, Cambridge, 2011).

⁶M. Kono and M. Skorić, Nonlinear Physics of Plasmas (Springer-Verlag, Heidelberg, 2010).

⁷E. P. Gross, "Structure of a quantized vortex in boson systems," Il Nuovo Cimento (1955-1965) 20, 454-477 (1961).

⁸L. P. Pitaevskii, "Vortex lines in an imperfect Bose gas," Sov. Phys. JETP 13(2), 451-454 (1961).

⁹L. Pitaevskii and S. Stringari, Bose-Einstein Condensation and Superfluidity (Oxford University Press, Oxford, 2015).

10 S. Cornish, N. Claussen, J. Roberts, E. Cornell, and C. Wieman, Phys. Rev. Lett. 85, 1795 (2000).

¹¹ K. Strecker, G. Partridge, A. Truscottand, and R. Hulet, Nature 417, 150 (2001). 12 L. Landau and E. Lifshitz, Quantum Mechanics: Non-Relativistic Theory, Vol. 3 (Butterworth-Heinemann, Boston, 2003).

13 E. G. Charalampidis, P. G. Kevrekidis, D. J. Frantzeskakis, and B. A. Malomed, "Dark-bright solitons in coupled nonlinear Schrödinger equations with unequal dispersion coefficients," Phys. Rev. E 91, 012924 (2015).

¹⁴E. G. Charalampidis, P. G. Kevrekidis, D. J. Frantzeskakis, and B. A. Malomed, "Vortex-soliton complexes in coupled nonlinear Schrödinger equations

with unequal dispersion coefficients," Phys. Rev. E 94, 022207 (2016).

15 E. Allgower and K. Georg, Numerical Continuation Methods: An Introduction, Vol. 13 (Springer-Verlag, Berlin, 1990).

16 B. Malomed and Y. Stepanyants, "The inverse problem for the Gross-Pitaevskii equation," Chaos 20, 01313 (2010).

¹⁷F. Cooper, A. Khare, S. Charalampidis, J. Dawson, and A. Saxena, "Stability of exact solutions of the (2 + 1)-dimensional nonlinear Schrödinger equation with arbitrary nonlinearity parameter κ ," Phys. Scr. 98, 015011 (2022).

¹⁸F. Cooper, A. Khare, J. F. Dawson, E. G. Charalampidis, and A. Saxena, "Uniform-density Bose-Einstein condensates of the Gross-Pitaevskii equation found by solving the inverse problem for the confining potential," Phys. Rev. E 107, 064202 (2023).

¹⁹G. H. Derrick, "Comments on nonlinear wave equations as models for elementary particles," J. Math. Phys. 5, 1252-1254 (1964).

²⁰N. N. Bogolyubov, "On the theory of superfluidity," J. Phys. (USSR) 11, 23–32 (1947).

²¹P. G. de Gennes, Superconductivity of Metals and Alloys, Vol. 86 (Benjamin, New York, 1966).

²²A. Gaidoukov and J. Anglin, "Bogoliubov-de Gennes theory of the snake instability of gray solitons in higher dimensions," Phys. Rev. A 103, 013319

²³J. Satsuma and N. Yajima, "B. Initial value problems of one-dimensional selfmodulation of nonlinear waves in dispersive media," Prog. Theor. Phys. Suppl. 55, 284-306 (1974).

²⁴H. F., "New development in freefem++," J. Numer. Math. **20**, 251–266 (2012).

²⁵R. B. Lehoucq, D. C. Sorensen, and C. Yang, *ARPACK Users' Guide* (Society for Industrial and Applied Mathematics, 1998).

15 April 2024 19:39:13